metals

MDPI

Article

Effects of MoO_3 + C on Crystallization and Radiative Heat Transfer of $CaO–SiO_2–B_2O_3$-Based Glassy Fluoride-Free Mold Fluxes

Qifeng Shu [1,2,*], Qiangqi Li [2] and Timo Fabritius [1]

[1] Process Metallurgy Research Unit, University of Oulu, FI-90014 Oulu, Finland; timo.fabritius@oulu.fi
[2] University of Science and Technology Beijing, Beijing 100083, China; ustbli2016@163.com
* Correspondence: qifeng.shu@oulu.fi; Tel.: +358-41-3197728

Received: 8 April 2019; Accepted: 29 April 2019; Published: 2 May 2019

Abstract: The fluorine in traditional mold fluxes could be harmful in steel-plant environments. Accordingly, fluoride-free mold fluxes have received great attention in recent years. In this work, a method to adjust the crystallization and radiative heat transfer of fluoride-free mold fluxes is proposed. MoO_3 and C mixtures (mass ratio: 4:1) were added into $CaO–SiO_2–B_2O_3$-based mold fluxes and produced MoB, Mo_2CB and Mo_2C foreign particles. The influences of foreign particles on the radiation of glassy $CaO–SiO_2–B_2O_3$-based mold fluxes were investigated by measuring the transmissivity of a glassy disk for light in the wavenumber range of 300 to 2500 nm. It was found that transmissivity in all wavenumber ranges were reduced and extinction coefficients were enhanced by the scattering of foreign particles. The effect of foreign particles on crystallization (devitrification) of bulk glassy $CaO–SiO_2–B_2O_3$-based mold fluxes was also investigated. The crystallization mechanism of glassy mold fluxes disks is mainly surface crystallization. The introduction of foreign particles induced heterogeneous nucleation and the crystallization mechanism of the bulk sample with MoO_3% = 2% changed into bulk crystallization.

Keywords: fluoride-free mold fluxes; radiative heat transfer; crystallization; particles in glass

1. Introduction

Mold fluxes are fed from the top of molten steel and then infiltrate into the gap between mold and steel strands during continuous casting [1]. Multiple layers, including glassy, crystalline and liquid layers, could be found between the mold and steel shell. One of the most important functions for mold fluxes is to provide optimal horizontal heat transfer. Multiple flux layers could be employed to tailor the horizontal heat transfer. For some steel grades, e.g., medium carbon steel, mild cooling should be maintained to avoid longitudinal surface cracks on the slabs [2]. It is well accepted that increasing crystallinity in the solid layer is the most effective way to increase the effective heat resistance between the mold and the steel shell [3,4]. There are two mechanisms by which the crystallization increases the heat resistance across the mold fluxes' layers [5]: (1) the crystallization of mold fluxes would increase the surface roughness of solid layers [6] and thereby promote the formation of an air gap between the mold and solid layer, which increase the interfacial thermal resistance [7]; (2) crystallizations would lower the transmissivity of flux layer and reduce the radiative heat transfer across the layer [8–10]. Therefore, the overall heat resistances are enhanced. It was reported that high-basicity mold fluxes could have stronger crystallization ability and be suitable for the casting of medium carbon steel [11].

The fluorine in traditional mold fluxes could be harmful to steel-plant environments and could even be leached into groundwater [12]. Accordingly, fluoride-free mold fluxes have received great attention in recent years. $CaO–SiO_2–TiO_2$-based mold fluxes [13–15] are considered to be potential

fluoride mold fluxes to replace traditional mold fluxes, with $CaTiO_3$ and $CaTiSiO_5$ being substitutes for cuspidine in mold fluxes. However, the lubrication functions of $CaO–SiO_2–TiO_2$-based mold fluxes still need to be improved [16]. Recently, $CaO–SiO_2–B_2O_3$-based mold fluxes were proposed by many researchers to be the most promising fluoride-free mold fluxes [17–20]. Industrial trials have been successfully made on continuous castings of steel billets and slabs [18,19]. Boron oxide could improve the lubrication function of mold fluxes. However, it is reported that boron oxide in fluoride-free mold fluxes would impair the crystallization ability of mold fluxes [21], which makes this kind of fluoride-free mold fluxes unsuitable for casting some crack-sensitive steel grades.

The introductions of foreign particles into glass to modify the crystallization and optical properties of glass were investigated by many researchers [22–24]. It is a well-accepted practice in glass ceramics technology to introduce some nucleating agents to provoke internal crystallization [22]. These nucleating agents could be metallic particles or some oxides, e.g., TiO_2, ZrO_2, etc. A new technology was proposed by researchers at Pohang University of Science and Technology to reduce the horizontal heat transfer across the mold fluxes by introducing metallic particles less than a few micrometers in glassy mold fluxes [23,24]. They explained the scattering of metallic particles in glass using Mie theory.

Inspired by these studies, foreign particles were introduced into fluoride-free mold fluxes by in situ reduction of MoO_3 with carbon in the present study. Several kinds of particles, e.g., MoB, formed during the melting of mold fluxes. These particles could scatter light and reduce radiative heat transfer. On the other hand, these particles could also provide potential sites for heterogeneous nucleation and promote the crystallization of fluoride-free mold fluxes. The promoted crystallization and suppressed radiative heat transfer could be beneficial to the application of fluoride-free mold fluxes in the casting some crack-sensitive steel grades.

To validate this idea, the transmissivity of mold fluxes disks with different MoO_3 + C contents were measured and extinction coefficients were calculated in the present work. In addition, the crystallization of mold fluxes with different MoO_3 + C contents were investigated by differential scanning calorimetry (DSC), scanning electron microscopy equipped with energy dispersive spectral (SEM-EDS) and X-ray diffraction (XRD).

2. Experimental Procedure

2.1. Sample Preparation

Reagent powders of $CaCO_3$, Al_2O_3, H_3BO_3, MoO_3, Na_2CO_3, SiO_2 and C were employed to prepare mold fluxes samples. The mass ratio of MoO_3 to C was set to be 4, which is the theoretical MoO_3/C ratio for following reaction: $MoO_3 + 3C = Mo + 3CO(g)$. $CaCO_3$ powders were heated at 1100 °C for 8 h in a muffle furnace to decompose into CaO. Al_2O_3, $Na2CO_3$ and SiO_2 powders were heated at 300 °C for 4 h to remove moisture. The reagent powders were mixed well in an agate mortar and put in a graphite crucible. The melting of mold fluxes was performed in a vertical tube furnace with $MoSi_2$ heating elements. To protect the oxidation of crucibles and samples, the furnace tube was purged by argon (purity > 99.999%). After melting, fluxes in crucibles were poured and quenched in an iron plate. The glassy samples were machined into a thin disk with a thickness of 3.5 mm. Chemical compositions (mass%) of the investigated mold fluxes are shown in Table 1. A part of the quenched samples was ground to fine powders and subjected to XRD. Another part of the quenched samples was coated with gold, and then subjected to SEM-EDS examination. SEM-EDS examinations were carried out using an FEI MLA 250 (Thermo Fisher, Waltham, MA, United States) unit equipped with Bruker SDD-detector (Bruker, Billerica, MA, USA) for EDS analyses. The working voltage was 20 kV. XRD analyses were performed on an 18 kW X-ray diffractometer (model: RIGAKU TTRIII, Rigaku, Tokyo, Japan) with Cu-Kα radiation.

Table 1. Chemical composition of the studied slag system.

Sample No.	Chemical Composition (wt. %)						
	CaO	**SiO_2**	**B_2O_3**	**Na_2O**	**Al_2O_3**	**MoO_3**	**C**
1	39.000	39.000	10.00	8.0	4.0	0	0.0
2	38.025	38.025	9.75	7.8	3.9	2	0.5
3	37.050	37.050	9.50	7.6	3.8	4	1.0
4	36.075	36.075	9.25	7.4	3.7	6	1.5

2.2. Radiation Experiment

The glassy disks were polished and then subjected to the radiation experiment. Transmittances of samples were measured by using an Ultraviolet-Visible-Near Infrared spectrophotometer (UV-Vis-NIR, Lambda750, Perkin-Elmer, Waltham, MA, United States) with an integrating sphere. The wavelength range of measurements was from 300 to 2500 nm. All measurements were performed at room temperature in air. Cho et al. [4] measured transmittances of disk mold fluxes samples at 300~773 K in a high-temperature cell using a Flourier transformation infrared (FT-IR) spectrometer. They found little change of shape and height of absorption, indicating that there is no large difference between high-temperature and room-temperature spectra.

2.3. Crystallization Experiments

Differential scanning calorimetry was employed to determine the crystallization temperature of samples during heating. The samples were pulverized and subjected to the DSC using argon as a purge gas with a thermal analyzer (STA 409C, Netzsch-Gerätebau GmbH, Selb, Germany). The samples were heated to 1350 °C with a heating rate of 20 K/min in a corundum crucible, using alfa-Al_2O_3 as a reference material. Approximately 25 mg of the powder sample was employed for each DSC run. Before measurements, temperature calibration, sensitivity calibration and balance calibration were performed.

To investigate the mechanism of crystallization of mold fluxes, quenched disk samples No. 1 and No. 2 were heated to crystallization temperature (peak temperatures for crystallization peaks) and soaked for 2 h. Then the samples were quenched in air and cut in perpendicular direction. Then these heat-treated samples were embedded with resin. The sections were ground and polished. After sections were coated with gold, the samples were subject to SEM-EDS examination. Parts of the samples were crushed and ground into fine powder and subjected to XRD measurement.

3. Results and Discussion

3.1. Microstructure of Samples

The micrographs of prepared disk samples are shown in Figure 1. The XRD patterns of powdered samples are shown in Figure 2. As can be seen in Figure 1, the Mo-free sample is homogeneous. No crystals but a glassy matrix was found in micrographs of the Mo-free sample. With the addition of MoO_3 and C, there were many particles found in micrographs of samples 2, 3 and 4. The particles agglomerated and formed large clusters. In the sample with MoO_3 = 2%, there were still many isolated spherical particles apart from clusters. The agglomeration of particles was promoted by increasing MoO_3 content and some coarser particles formed due to the agglomeration and growth of particles. There were no crystals found in all disk samples with MoO_3 + C addition, indicating that no crystallization took place during quenching.

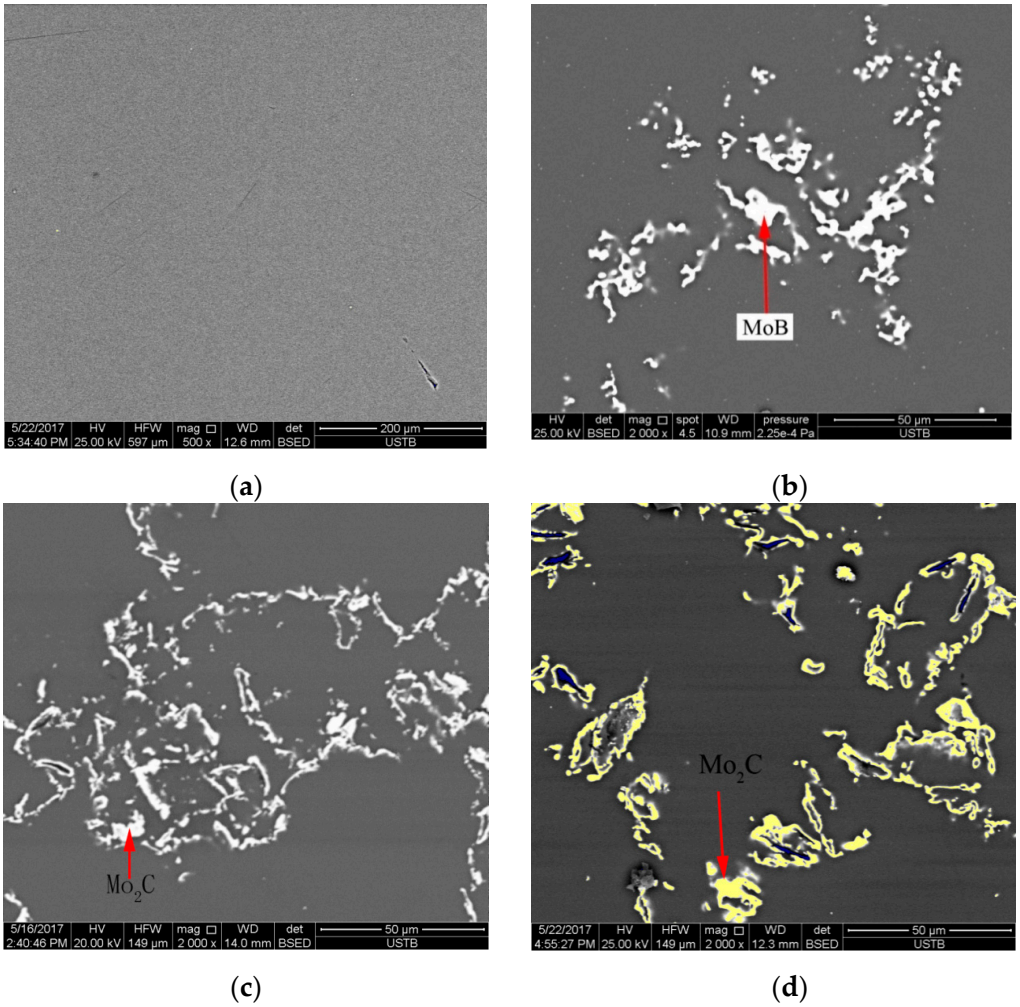

Figure 1. Micrographs of disk samples with different MoO_3 content levels: (**a**) MoO_3% = 0%; (**b**) MoO_3% = 2%; (**c**) MoO_3% = 4%; (**d**) MoO_3% = 6%.

Combining EDS results with the XRD pattern in Figure 2, the particle phases in micrographs could be determined. For the sample with MoO_3 = 2%, EDS showed a chemical composition of particles contains B and Mo. XRD confirmed that there was only one crystalline phase, MoB, in the sample with MoO_3 = 2%. MoB has a very high melting point of 2873 K [25], and this persisted in a solid state during the melting of mold fluxes. The possible reaction for formation of MoB could be as follows:

$$9C + 2MoO_3 + B_2O_3 = 2MoB + CO(g). \quad (1)$$

With increasing MoO_3 addition, there was C found in the EDS results of samples. XRD showed that the particle phases were shifted from MoB to Mo_2BC and Mo_2C. The melting point of Mo_2C is 2793 K [26] and the melting point of Mo_2BC is 3073 K [27]. These compounds were also solid during the melting of the studied slag system. The formation of Mo_2BC could be due to the following reaction:

$$17C + 4MoO_3 + B_2O_3 = 2Mo_2BC + 15CO(g). \quad (2)$$

The possible reaction for Mo2C formation could be as follows:

$$14C + 4MoO_3 = 2Mo_2C + 12CO(g). \quad (3)$$

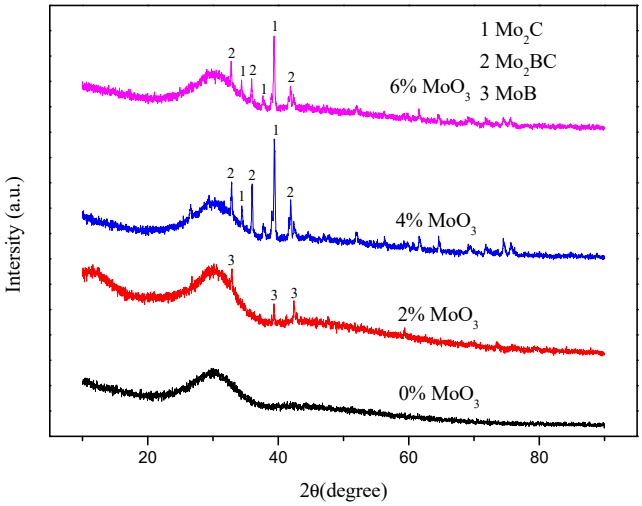

Figure 2. X-ray diffraction (XRD) patterns of disk samples with different MoO_3 contents.

3.2. Radiation Properties of Samples

Results from the transmittance measurements are shown in Figure 3. It can be clearly observed that transmissivities in all wavenumber ranges were heavily reduced by the introduction of Mo-containing particles. The reduction of transmittance by Mo addition became mild with the further addition of 6% MoO_3. The extinction coefficients of various samples could be calculated from transmittance values by employing the Lambert–Beer law:

$$\tau = \exp(-Ed) \tag{4}$$

where E is the extinction coefficient of the sample; d is the thickness of the sample; τ is the transmittance of the sample.

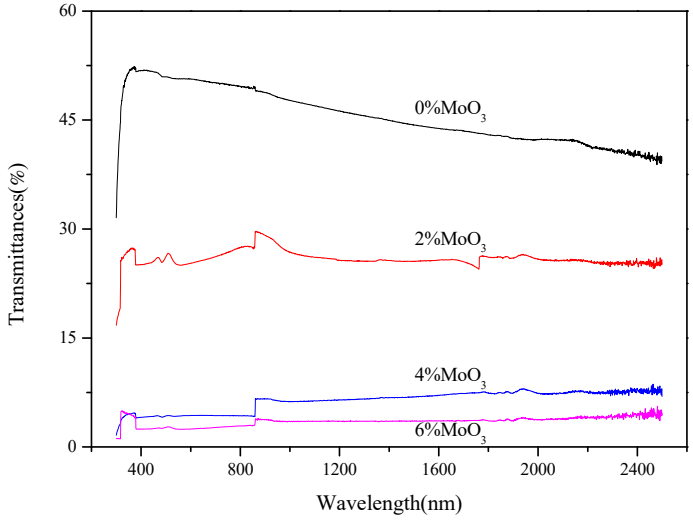

Figure 3. The transmittances of samples with various MoO_3 contents.

The calculated extinction coefficients of various samples are shown in Figure 4. Strong absorptions below 400 nm were found in all samples, which could be associated with a charge transfer band [10]. There are some new peaks around 400–600, 800–900 and 1600–2000 nm found in samples with MoO_3 addition, which could be due to the introduction of MoO_3 in the structure of glass [28]. The Mo-free sample had extinction coefficient values between 150 and 300 m^{-1}. The extinction coefficients from the Mo-free sample correspond to the lowest values in the references [23]. This is due to the fact that

there were minor transition metal oxides, e.g., Fe_2O_3, in the composition of glasses reported in the references [23]. The transition metal oxides could increase the apparent absorptivity and decrease the apparent reflectivity, thereby increasing the absorption and extinction coefficients [29]. With the introduction of foreign particles, the extinction coefficients could be enhanced to near 1000 m^{-1}. The extinction coefficients increased with increasing MoO_3 content in the samples, indicating that the scattering due to particles was enhanced.

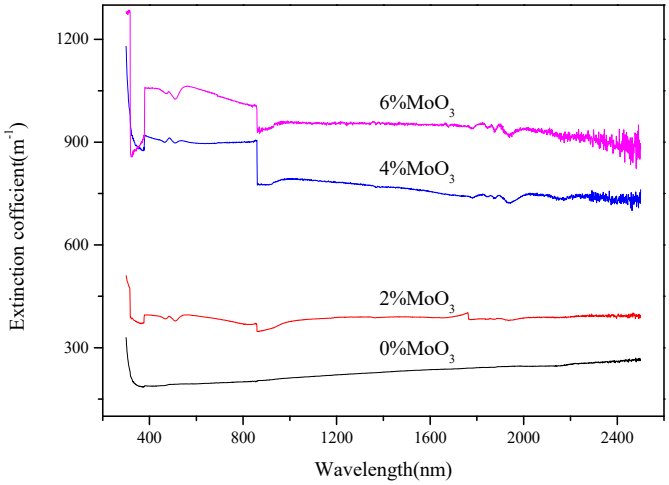

Figure 4. The calculated extinction coefficients of samples with various MoO_3 contents.

Yoon et al. [23,24] measured the extinction coefficients of mold fluxes containing iron metallic particles and found that the extinction coefficients were enhanced by the scattering of iron particles. They employed Mie's theory [30] to calculate the scattering coefficients and the calculated values were found to be in good agreement with the measured values. In the present work, the extinction coefficients were also enhanced by the scattering of particles. However, there are some differences between the present work and Yoon's work. The sizes of particles in the present work are larger than those in Yoon's work. In particular, large particle clusters were found in the samples with the addition of MoO_3 + C. Mie's theory could only be applied to light scattering by particles whose size is comparable with the wavelength of the incident light. Due to the larger size and agglomeration of crystals, the quantification of scattering due to particles by using Mie's theory is difficult. However, the qualitative explanation of the extinction coefficient change due to the scattering of particles could be given by employing Mie's theory. The scattering coefficient (μ_{scat}) could be calculated from the total scattering cross-section (σ_{scat}) [23]:

$$\mu_{scat} = \rho_s \sigma_{scat} \tag{5}$$

where ρ_s is the density of spherical particles in the glassy matrix.

The total scattering cross-section (σ_{scat}) could be calculated in terms of Mie's theory:

$$\sigma_{scat} = \frac{\lambda^2}{2\pi} \sum_{n=0}^{\infty} (2n+1)\left(|a_n|^2 + |b_n|^2\right) \tag{6}$$

where a_n and b_n are parameters defined as:

$$a_n = \frac{\psi_n(x)\psi_n'(mx) - m\psi_n(mx)\psi_n'(x)}{\xi_n(x)\psi_n'(mx) - m\psi_n(mx)\xi_n'(x)} \tag{7}$$

$$b_n = \frac{m\psi_n(x)\psi_n'(mx) - \psi_n(mx)\psi_n'(x)}{m\xi_n(x)\psi_n'(mx) - \psi_n(mx)\xi_n'(x)} \tag{8}$$

where ψ_n and ξ_n are Ricatti–Bessel functions. x is the particle size parameter which is the ratio of the subsidence perimeter of the spherical particle to the frequency of the incident beam in the medium:

$$x = \frac{2\pi r n_{\text{med}}}{\lambda} \tag{9}$$

where r is the particle radium; n_{med} is the refractive index in the medium; λ is the wavelength of the incident rays.

It could be seen from Equation (5) that the scattering coefficient is proportionate to the density of spherical particles. In the present samples, with increasing MoO_3 content, as can be seen in Figure 1, the number of particles increased. Accordingly, the scattering coefficient increased with increasing MoO_3 content. The extinction coefficient includes contributions from scattering and absorption. Since the composition of the base glass is the same, absorption coefficients of different samples are fixed. Therefore, with increasing MoO_3 content, the extinction coefficient of samples increases.

3.3. Crystallization of Samples

The DSC curves for the powder Mo-free sample and the powder sample with MoO_3 = 2% are shown in Figure 5. After the step for glass transition, an exothermic thermal peak could be found in each curve, which was due to the crystallization of the glassy sample. The glass transition temperatures T_g for the Mo-free sample and sample with MoO_3 = 2% were obtained as the temperature at half the step height in the DSC curves. The crystallization temperatures of samples T_c were determined as the peak position of the crystallization event. Thermal stability, $T_c - T_g$, could be employed to measure the crystallization ability of the sample. The larger the $T_c - T_g$ value, the weaker the crystallization ability. The $T_c - T_g$ values for the Mo-free sample and the sample with MoO_3 = 2% were 77.9 and 73.5 °C, respectively, which are close to each other. This indicates that the two powder samples have near crystallization ability.

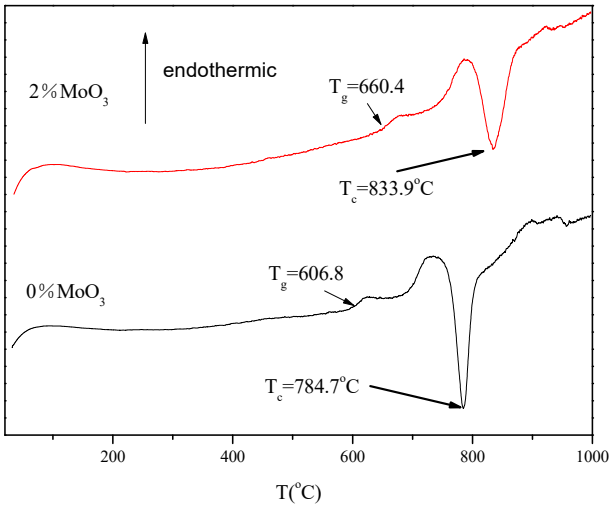

Figure 5. Differential scanning calorimetry (DSC) curves of samples during heating.

The bulk Mo-free sample and the sample with MoO_3 = 2% were heated at the crystallization temperature determined by DSC for 2 h and quenched. The XRD patterns for samples are shown in Figure 6. It could be seen that only one kind of crystal, $CaSiO_3$, precipitated from all glassy samples. The ratios of CaO to SiO_2 for all samples were equal to 1. According to the phase diagram of $CaO–SiO_2–B_2O_3$ [31], the compositions of the present fluxes were within the primary crystal field of $CaSiO_3$. Therefore, the firstly precipitated crystals should be $CaSiO_3$. In our previous work on the crystallization of $CaO–SiO_2–B_2O_3$ [15], the crystallization product was also $CaSiO_3$, which is in line with the present work. It could be also seen that the crystalline peaks in the XRD pattern of the sample

with MoO_3 = 2% were much sharper than those of the Mo-free sample. All these indicate that the crystallization of mold fluxes was promoted by the addition of 2% MoO_3.

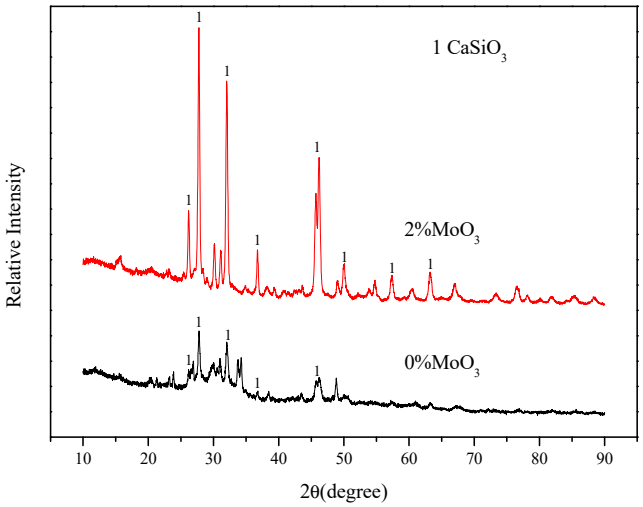

Figure 6. XRD patterns of samples heated at the crystallization temperature.

The micrographs of the Mo-free sample and the sample with MoO_3 = 2% are shown in Figures 7 and 8. In the micrograph of the Mo-free sample, it can clearly be seen that crystal nucleation and growth can be started from the edge of the sample, which corresponds to the surface of the sample. In enlarged micrographs, columnar crystals could be easily found. The growth direction for all crystals is from the edge to the inner part of the sample. The compositions of crystals were determined by EDS to be $CaSiO_3$, which is consistent with the XRD results. In most of the inner part of sample, there were no crystals found. All these indicate that the main crystallization mechanism for Mo-free samples could be surface crystallization. Surface crystallization was frequently found to be the crystallization mechanism for glass [32] and glassy mold fluxes [15,33]. Wang et al. [33] investigated the crystallization kinetic of glassy mold fluxes with different TiO_2 contents and suggested that the crystallization mechanism for all samples should be surface crystallization.

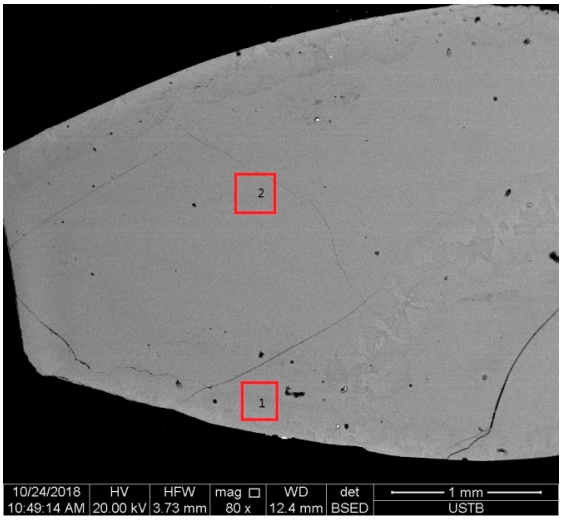

(a)

Figure 7. *Cont.*

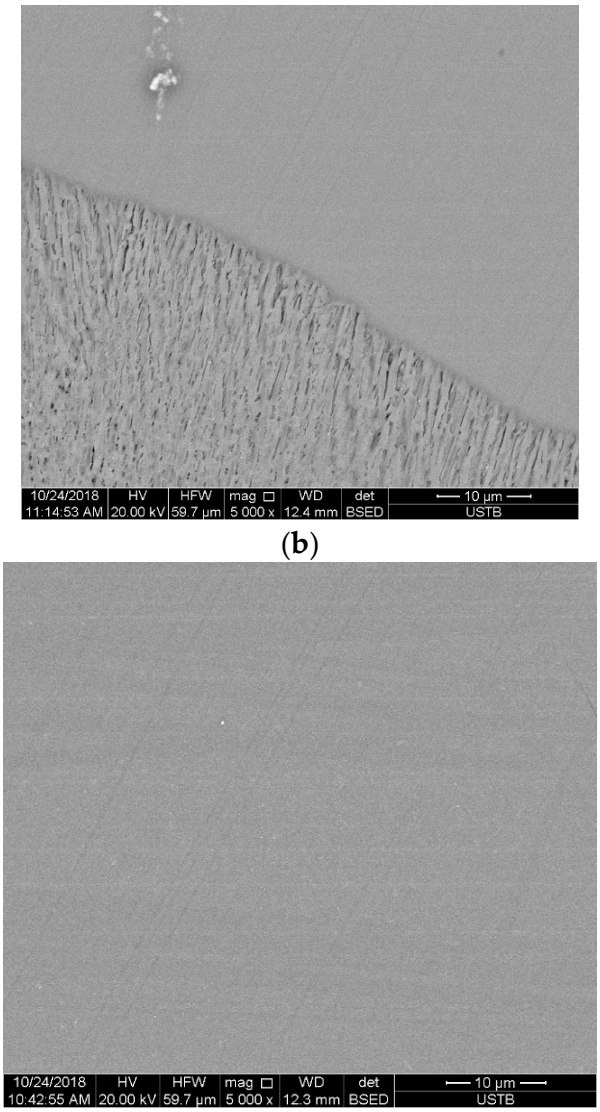

Figure 7. The micrographs of MoO_3-free samples: (**a**) low-magnification micrograph; enlarged micrographs of (**b**) zone 1 and (**c**) zone 2.

The micrographs of the sample with MoO_3 = 2% showed MoB clusters and many strip-like crystals. The EDS analysis showed that the composition of the strip-like crystals was $CaSiO_3$. The crystallization of CaO–SiO_2–B_2O_3 with various TiO_2 contents was investigated by DTA and SEM-EDS [15]. Stripe-like $CaSiO_3$ crystals were also found in all samples. The strip-like morphology of $CaSiO_3$ could be found in natural minerals. It is well known that $CaSiO_3$ has a linear chain-like structure. The strip-like crystals of $CaSiO_3$ may stem from its chain-like structural characteristic.

The sample with MoO_3 = 2% was well crystallized and very few glass matrices could be found. This indicates that the crystallinity of the sample with MoO_3 = 2% was much higher than that of the Mo-free sample. In addition, the crystal number and size in the sample with MoO_3 = 2% were much higher than those in the Mo-free sample, indicating that the nucleation and growth of crystals were promoted by the addition of Mo-containing particles. It is possible that there were some bubbles on the surface of the samples, which could also be beneficial to the nucleation of crystals. Crystals could be found not only in the edge (surface) but everywhere in the inner part of the sample with MoO_3 = 2%. This means that the crystallization mechanism of the sample with MoO_3 = 2% was

critically altered. The crystallization mechanism was changed from surface nucleation and growth to internal crystallization.

Both surface crystallization and bulk crystallization could be found during the devitrification of glass. Zanotto et al. [32] pointed out that only glass systems that have $T_g/T_L < 0.58$ (T_g: glass transition; T_L: liquidus temperature) display measurable internal nucleation rates on a laboratory time-scale. It is a common practice in glass science to add some foreign particles or other nucleating agents to induce internal crystallization for the fabrication of glass ceramics. Heterogeneous nucleation fabricated by nucleating agents is usually responsible for the required internal crystallization [22].

When the melt contains solid particles or is in contact with a crystalline crucible or oxide layers, nucleation may be facilitated, which is known as heterogeneous nucleation [34]. Nucleation could be greatly facilitated by an area of low-energy solid/solid interface. The magnitude of the effect $f(\theta)$ could be calculated as a function of the contact angle, θ:

$$f(\theta) = \frac{(2 + \cos\theta)(1 - \cos\theta)^2}{4}. \quad (10)$$

The contact angle θ in Equation (10) is the contact angle between solid nuclei and solid particles with the presence of melts. However, it is difficult to obtain the contact angle due to significant data limitations. According to the theory advanced by Turnbull and Vonnegut [35,36], a nucleating agent will be effective in promoting nucleation when the lattice parameters in the low-index crystallographic planes of both the substrate and the nucleated solid are similar. The precipitated $CaSiO_3$ crystal is mainly pseudowollastonite and has a triclinic symmetry (JCPDS-PDF, card No. 74-874). However, the degrees of the three angles are approaching 90°. The lattice parameters are a = 6.85300, b = 11.89500 and c = 19.67400. The MoB particles have a tetragonal symmetry and lattice parameters of $a = b$ = 3.11245, c = 16.9560 (JCPDS-PDF, card No. 51-940). It was found that the c parameter of MoB is close to that of $CaSiO_3$, indicating that MoB could be effective in provoking heterogeneous nucleation.

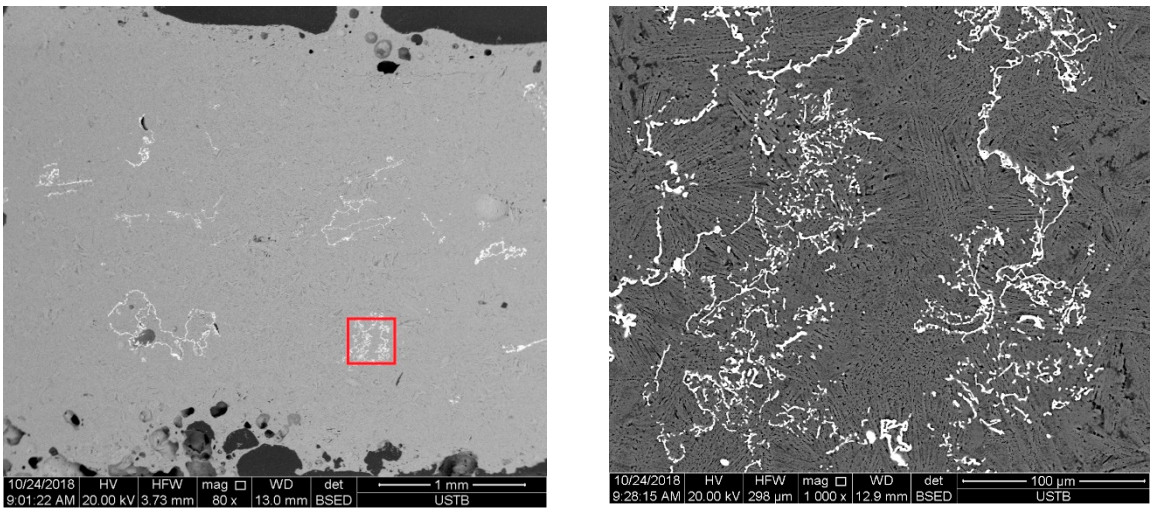

(**a**) (**b**)

Figure 8. The micrographs of samples with MoO_3% = 2%: (**a**) low-magnification micrograph; (**b**) enlarged micrographs.

It seems that the promotion of crystallization by MoO_3 + C in the bulk sample is inconsistent with the observation in DSC. This could be due to the different nature of samples. In the powder sample investigated by DSC, due to fine size and defects caused by crushing, the crystallization mechanism could be totally different from the bulk sample. It was reported that an even particle size of the powdered samples would influence the crystallization mechanism of glass determined by DSC [37].

It was observed that the introduction of MoO_3 + C would decrease the extinction coefficients of fluoride-free mold fluxes. The radiative heat transfer of the glassy layer would be weakened by the scattering of Mo-containing particles. On the other hand, the introduction of MoO_3 + C would also promote the crystallization of mold fluxes. The enhanced crystallization of mold fluxes would also weaken the radiative heat transfer of mold fluxes by the scattering of precipitated crystals. Moreover, the well-developed crystalline layer would increase the interfacial thermal resistances. In conclusion, the introduction of MoO_3 + C would weaken the heat transfer between the mold and the steel shell, and therefore lead to mild cooling, which is beneficial for the continuous casting of some crack-sensitive steel grades.

4. Conclusions

MoO_3 and C mixtures (mass ratio: 4:1) were introduced into CaO–SiO_2–B_2O_3-based mold fluxes to adjust the radiative and crystallization of fluoride-free mold fluxes. The influences of particles on the radiative and crystallization of glassy CaO–SiO_2–B_2O_3-based mold fluxes were investigated by UV-Vis-NIR, DSC, XRD and SEM-EDS. The following conclusions could be drawn:

(1) Particles of MoB, Mo_2BC and Mo_2C with very high melting temperatures could be generated by carbon reduction in mold fluxes. The particles collided and agglomerated into clusters.
(2) Transmittances in all wavenumber ranges were heavily reduced by the introduction of Mo-containing particles. With the addition of Mo-containing particles, the calculated extinction coefficients were enhanced.
(3) Both the Mo-free sample and the sample with MoO_3 = 2% precipitated $CaSiO_3$ crystals. The crystallization of fluxes was promoted by the introduction of Mo-containing particles.
(4) The crystallization mechanism for the Mo-free sample is mainly surface nucleation and growth. The introduction of Mo-containing particles facilitates heterogeneous nucleation, and the crystallization mechanism changes from surface nucleation and growth to internal nucleation and growth.

Author Contributions: Q.S. designed the experiments and wrote the paper; Q.L. performed experiments and plotted some figures; T.F. provided some discussions on the experiments and revised the paper.

Acknowledgments: Financial support from the Academy of Finland for Genome of steel grant (No. 311934) and Natural Science Foundation of China (NSFC contract no.51774026) is gratefully acknowledged.

Conflicts of Interest: The authors declare no conflict of interest.

References

1. Mills, K.C.; Fox, A.B. The Role of Mould Fluxes in Continuous Casting-So Simple yet So Complex. *ISIJ Int.* **2007**, *43*, 1479–1486. [CrossRef]
2. Hanao, M.; Kawamoto, M.; Yamanaka, A. Influence of mold flux on initial solidification of hypo-peritectic steel in a continuous casting mold. *ISIJ Int.* **2012**, *52*, 1310–1319. [CrossRef]
3. Cho, J.W.; Emi, T.; Shibata, H.; Suzuki, M. Heat transfer across mold flux film in mold during initial solidification in continuous casting of steel. *ISIJ Int.* **1998**, *38*, 834–842. [CrossRef]
4. Cho, J.; Shibata, H.; Emi, T.; Suzuki, M. Radiative heat transfer through mold flux film during initial solidification in continuous casting of steel. *ISIJ Int.* **1998**, *38*, 268–275. [CrossRef]
5. Nakada, H.; Susa, M.; Seko, Y.; Hayashi, M.; Nagata, K. Mechanism of heat transfer reduction by crystallization of mold flux for continuous casting. *ISIJ Int.* **2008**, *48*, 446–453. [CrossRef]
6. Tsutsumi, K.; Nagasaka, T.; Hino, M. Surface roughness of solidified mold flux in continuous casting process. *ISIJ Int.* **1999**, *39*, 1150–1159. [CrossRef]
7. Yamauchi, A.; Sorimachi, K.; Sakuraya, T.; Fujii, T. Heat transfer between mold and strand through mold flux film in continuous casting of steel. *ISIJ Int.* **1993**, *33*, 140–147. [CrossRef]
8. Taylor, R.; Mills, K.C. Physical properties of casting powders: Part 3. Thermal conductivities of casting powders. *Ironmak. Steelmak.* **1988**, *15*, 187–194.

9. Susa, M.; Li, F.; Nagata, K. Determination of refractive index and absorption coefficient of iron- oxide-bearing slags. *Metall. Trans. B* **1992**, *23*, 331–337. [CrossRef]
10. Ozawa, S.; Susa, M.; Goto, T.; Endo, R.; Mills, K.C. Lattice and radiation conductivities for mould fluxes from the perspective of degree of crystallinity. *ISIJ Int.* **2006**, *46*, 413–419. [CrossRef]
11. Hanao, M. Influence of basicity of mold flux on its crystallization rate. *ISIJ Int.* **2013**, *53*, 648–654. [CrossRef]
12. Shilov, A.; Holappa, L. Mass Spectrometric Measurements of the Gas Phase Composition over Mould Powder Samples in Vacuum Conditions at 50–1550 °C. *Steel Res. Int.* **2006**, *77*, 803–808. [CrossRef]
13. Nakada, H.; Nagata, K. Crystallization of CaO–SiO_2–TiO_2 slag as a candidate for fluorine free mold flux. *ISIJ Int.* **2006**, *46*, 441–449. [CrossRef]
14. Wen, G.; Sridhar, S.; Tang, P.; Qi, X.; Liu, Y. Development of fluoride-free mold powders for peritectic steel slab casting. *ISIJ Int.* **2007**, *47*, 1117–1125. [CrossRef]
15. Wang, Z.; Shu, Q.; Chou, K. Crystallization Kinetics of CaO-SiO_2 (CaO/SiO_2 = 1)-TiO_2-10 mass% B_2O_3 Glassy Slag by Differential Thermal Analysis. *ISIJ Int.* **2015**, *55*, 709–716. [CrossRef]
16. Wang, Q.; Lu, Y.J.; He, S.P.; Mills, K.C.; Li, Z.S. Formation of TiN and Ti (C, N) in TiO_2 containing, fluoride free, mould fluxes at high temperature. *Ironmak. Steelmak.* **2011**, *38*, 297–301. [CrossRef]
17. Choi, S.Y.; Lee, D.H.; Shin, D.W.; Choi, S.Y.; Cho, J.W.; Park, J.M. Properties of F-free glass system as a mold flux: Viscosity, thermal conductivity and crystallization behavior. *J. Non-Cryst. Solids* **2004**, *345–346*, 157–160. [CrossRef]
18. Fox, A.B.; Mills, K.C.; Lever, D.; Bezerra, C.; Valadares, C.; Unamuno, I.; Laraudogoitia, J.J.; Gisby, J. Development of fluoride-free fluxes for billet casting. *ISIJ Int.* **2005**, *45*, 1051–1058. [CrossRef]
19. Klug, J.L.; Pereira, M.M.; Nohara, E.L.; Freitas, S.L.; Ferreira, G.T.; Jung, D. F-free mould powders for low carbon steel slab casting–technological parameters and industrial trials. *Ironmak. Steelmak.* **2016**, *43*, 559–563. [CrossRef]
20. Zhou, L.; Wang, W.; Wei, J.; Zhou, K. Melting and heat transfer behavior of fluorine-free mold fluxes for casting medium carbon steels. *ISIJ Int.* **2015**, *55*, 821–829. [CrossRef]
21. Shu, Q.; Wang, Z.; Klug, J.L.; Chou, K.; Scheller, P.R. Effects of B_2O_3 and TiO_2 on Crystallization Behavior of Slags in Al_2O_3–CaO–MgO–Na_2O–SiO_2 System. *Steel Res. Int.* **2013**, *84*, 1138–1145. [CrossRef]
22. Holand, W.; Beall, G.H. *Glass Ceramic Technology*; John Wiley & Sons: Hoboken, NJ, USA, 2012.
23. Yoon, D.W.; Cho, J.W.; Kim, S.H. Scattering Effect of Iron Metallic Particles on the Extinction Coefficient of CaO-SiO_2-B_2O_3 -Na_2O-Fe_2O_3 -CaF_2, Glasses. *Metall. Mater. Trans. B* **2016**, *47*, 1–8. [CrossRef]
24. Yoon, D.W.; Cho, J.W.; Kim, S.H. Controlling radiative heat transfer across the mold flux layer by the scattering effect of the borosilicate mold flux system with metallic iron. *Metall. Mater. Trans. B* **2017**, *48*, 1951–1961. [CrossRef]
25. Spear, K.E.; Liao, P.K. The B–Mo (Boron-Molybdenum) system. *J. Phase Equilib.* **1988**, *9*, 457–466. [CrossRef]
26. Predel, B. C-Mo (Carbon-Molybdenum). In *B-Ba–C-Zr. Landolt-Börnstein-Group IV Physical Chemistry (Numerical Data and Functional Relationships in Science and Technology)*; Madelung, O., Ed.; Springer: Berlin/Heidelberg, Germany, 1992; Volume 5b.
27. Rudy, E.; Benesovsky, F.; Toth, L. Studies of the ternary systems of the group Va and VIa metals with boron and carbon. *Z. Metallkd.* **1963**, *54*, 345–353.
28. Abo-Naf, S.M. FTIR and UV–VIS optical absorption spectra of gamma-irradiated MoO_3-doped lead borate glasses. *J. Non-Crystall. Solids* **2012**, *358*, 406–413. [CrossRef]
29. Diao, J.; Xie, B.; Xiao, J.; Ji, C. Radiative heat transfer in transition metal oxides contained in mold fluxes. *ISIJ Int.* **2009**, *49*, 1710–1714. [CrossRef]
30. Mie, G. Articles on the optical characteristics of turbid tubes, especially colloidal metal solutions. *Ann. Phys.* **1908**, *25*, 377–445. [CrossRef]
31. Kowalski, M.; Spencer, P.J.; Neuschutz, D. Phase diagrams. In *'Slag Atlas'*; Verlag Stahleisen GmbH: Duesseldorf, Germany, 1995; Volume 99, p. 119.
32. Zanotto, E.D.; Fokin, V.M. Recent studies of internal and surface nucleation in silicate glasses. *Philos. Trans. R. Soc. Lond. Ser. A: Math. Phys. Eng. Sci.* **2003**, *361*, 591–613. [CrossRef]
33. Wang, Z.; Shu, Q.; Chou, K. Crystallization kinetics and structure of mold fluxes with SiO_2 being substituted by TiO_2 for casting of titanium-stabilized Stainless Steel. *Metall. Mater. Trans. B* **2013**, *44*, 606–613. [CrossRef]
34. Kurz, W.; Fisher, D.J. *Fundamentals of Solidification*; Trans Tech Publications: Aedermannsdorf, Switzerland, 1986.

35. Turnbull, D.; Vonnegut, B. Nucleation catalysis. *Ind. Eng Chem.* **1952**, *44*, 1292–11298. [CrossRef]
36. Bramfitt, B.L. The effect of carbide and nitride additions on the heterogeneous nucleation behavior of liquid iron. *Metall. Trans.* **1970**, *1*, 1987–1995. [CrossRef]
37. Ray, C.S.; Huang, W.; Day, D.E. Crystallization kinetics of a lithia–silica glass: Effect of sample characteristics and thermal analysis measurement techniques. *J. Am. Ceram. Soc.* **1991**, *74*, 60–66. [CrossRef]